ELSEVIER

Journal of Organometallic Chemistry 633 (2001) 51–65

Journal of Organometallic Chemistry

www.elsevier.com/locate/jorganchem

# 47-Electron organometallic clusters derived by chemical and electrochemical oxidation of trihydrido(alkylidyne)triruthenium clusters
## II. Disproportionation mechanism for decomposition

David J. Bierdeman [a], Jerome B. Keister [a,*], Daniel A. Jelski [b,1]

[a] *Department of Chemistry, Natural Sciences Complex, State University of New York College at Buffalo, Buffalo, NY 14260-3000, USA*
[b] *Department of Chemistry, State University of New York College at Fredonia, Fredonia, NY 14063, USA*

Received 5 February 2001; received in revised form 14 May 2001; accepted 16 May 2001

**Abstract**

The decomposition of 47-electron clusters, generated by chemical or electrochemical oxidations of 48-electron $H_3Ru_3(\mu_3\text{-}CX)(CO)_{9-n}L_n$ (X = OMe; L = $PPh_3$; $n = 0$–3: X = OMe, SEt; L = dppm; L = $PPh_3$; $n = 3$: X = SEt, NMeBz; L = $PR_3$, $SbPh_3$; $n = 2,3$) occurs by disproportionation back to the 48-electron precursor and very unstable 46-electron species. Both 47/48- and 46/47-e redox potentials display similar ligand additivity trends, which are correlated with HOMO energies determined by Fenske–Hall MO calculations. Decomposition of $[H_3Ru_3(\mu_3\text{-}COMe)(CO)_6(PPh_3)_3]^{1+}$ in the presence of added $PPh_3$ forms 48-e $H_3Ru_3(\mu_3\text{-}COMe)(CO)_6(PPh_3)_3$, 46-e $[H_3Ru_3(CO)_7(PPh_3)_3]^{1+}$, and $[MePPh_3]^{1+}$; the rate law is second order with respect to concentration of the 47-e cluster and displays a small dependence on $PPh_3$ concentration. Decompositions of $[H_3Ru_3(\mu_3\text{-}COMe)(CO)_7(PPh_3)_2]^{1+}$, $[H_3Ru_3(\mu_3\text{-}CSEt)(CO)_7(dppm)]^{1+}$, and $[H_3Ru_3(\mu_3\text{-}CSEt)(CO)_6(PPh_3)_3]^{1+}$ are also second order, although only the 48-e product could be characterized. The mechanism is proposed to involve rate-limiting outer-sphere electron transfer, the slow rate of disproportionation is a consequence of the fact that the reaction involves transfer of an electron from one half-filled bonding orbital to another half-filled bonding orbital, thus requiring considerable reorganization energy. Electrochemical studies of the 2-e oxidations of $H_3Ru_3(\mu_3\text{-}COMe)(CO)_{9-n}(PPh_3)_n$, $n = 0$ and 1, indicate that the initial 46-e cluster rearranges very rapidly to a new 46-e species, which decomposes rapidly to electrochemically inactive products. 

*Keywords:* Ruthenium; Alkylidyne; Electrochemical oxidation; Electron transfer

## 1. Introduction

The importance of odd-electron organometallic intermediates is now well-appreciated [1–3]. One common pathway for decomposition of 17-electron organometallic radicals is nucleophile-assisted disproportionation; this reaction, which proceeds via an associative mechanism through a 19-electron intermediate, typically has a rate law which is first-order in 17-electron complex and first-order in the nucleophile [3]. On the other hand, disproportionations of the radicals $[M_2(CO)_{10}]^-$ (M = Cr, Mo, W), in which the SOMO is a metal–metal bonding orbital, proceed via rate-limiting electron transfer [4]. In recent years we have conducted systematic investigations of the electrochemistry of the related 48-electron cluster series $(\mu\text{-}H)_{3-m}Ru_3(\mu_3\text{-}(CR)_{m+1})(CO)_{9-n}(PR_3)_n$, $m = 0$–2, $n = 0$–3, and also their reactions with electrophile/oxidants [5–8]. The comparison of the 47-e clusters derived by 1-e oxidation showed that $[HRu_3(XCCRCR')(CO)_{9-n}L_n]^{1+}$ and $[H_2Ru_3(XCCR)(CO)_{9-n}L_n]^{1+}$, which have SOMOs of metal–metal bonding character, were much less stable than $[H_3Ru_3(CX)(CO)_{9-n}L_n]^{1+}$, for which the SOMO has metal–carbon bonding character.

* Corresponding author. Fax: +1-716-645-6963.
*E-mail address:* keister@ascu.buffalo.edu (J.B. Keister).
[1] Present address: Department of Chemistry, Rose-Hulman Institute of Technology, 5500 Wabash Avenue, Terre Haute, IN 47803, USA.

0022-328X/01/$ - see front matter 
PII: S0022-328X(01)01002-6

In this paper we present results of a study of the mechanism of decomposition of 47-electron $[H_3Ru_3(CX)(CO)_{9-n}L_n]^{1+}$, which occurs by slow disproportionation to the 48-e precursor and a very unstable and uncharacterized 46-e cluster. In the presence of $PPh_3$, the disproportionation of $[H_3Ru_3(COMe)(CO)_6(PPh_3)_3]^{1+}$ forms 46-e $[H_3Ru_3(CO)_7(PPh_3)_3]^{1+}$, 48-e $H_3Ru_3(COMe)(CO)_6(PPh_3)_3$, and $[MePPh_3]^{1+}$.

## 2. Experimental

### 2.1. Chemicals

$H_3Ru_3(CX)(CO)_{9-n}L_n$ (X = OMe, $n = 0$–3, L = $PPh_3$; X = SEt, $n = 3$, L = $PPh_3$; X = NMeBz, $n = 3$, L = $PPh_3$, $SbPh_3$) were prepared by previously published procedures [6,9–12]. The new complexes $H_3Ru_3(CSEt)(CO)_6(dppm)(PPh_3)$, $H_3Ru_3(CSEt)(CO)_7(dppm)$, $H_3Ru_3(COMe)(CO)_7(dppm)$, $H_3Ru_3(COMe)(CO)_6(dppm)(PPh_3)$, $H_3Ru_3(CNEtBz)(CO)_6(PPh_3)_3$, and $H_3Ru_3(CNEtBz)(CO)_6(PPh_3)_2(CNBz)$ were prepared in analogous procedures by substitution of the appropriate ligands. Spectroscopic characterizations of the new complexes are provided in Tables 1 and 2.

Table 1
IR data for new clusters

| Cluster | $\nu$ (CO) ($cm^{-1}$) |
|---|---|
| $H_3Ru_3(CSEt)(CO)_6(PPh_3)$-(dppm) [b] | 2034 w, 2014 s, 2006 m, 1971 sh w, 1964 m |
| $H_3Ru_3(CSEt)(CO)_7(dppm)$ | 2077 s, 2030 m, 2020 vs, 2012 s, 1995 w, 1978 m, 1976 w |
| $H_3Ru_3(COMe)(CO)_6$-$(PPh_3)(dppm)$ [b] | 2026 m, 2003 s, 1996 sh m, 1951 m, 1936 sh w |
| $H_3Ru_3(COMe)(CO)_7$-(dppm) [a] | 2072 s, 2011 vs, 1962 br w |
| $H_3Ru_3(COMe)(CO)_7$-(dppm)]$^+$ [a] | 2124 m, 2066 s, 2022 br s |
| $H_3Ru_3(CNMeBz)(CO)_7$-$(PPh_3)_2$ [a] | 2074 m, 2057 w, 2023 s, 2008 s, 1958 m |
| $H_3Ru_3(CNMeBz)(CO)_7$-$(PPh_3)_2$ | 2074 m, 2057 w, 2023 s, 2008 s, 1958 m |
| $H_3Ru_3(CNMeBz)(CO)_7$-$(PPh_3)_2]^+$ [a] | 2105 m, 2073 w, 2056 s, 2042 s, 2023 m, 2000 sbr, 1960 w |
| $H_3Ru_3(CNMeBz)(CO)_6$-$(PPh_3)_2(CNBz)$ | 2173 br m, 2008 s, 1993 s, 1968 br m, 1947 br m |
| $H_3Ru_3(CNEtBz)(CO)_6$-$(PPh_3)_3$ [a] | 2028 vs, 2004 m, 1997 s, 1951 m |
| $H_3Ru_3(CNEtBz)(CO)_6$-$(PPh_3)_3$ [b] | 2032 vs, 2011 m, 2003 s, 1958 m |
| $H_3Ru_3(CNEtBz)(CO)_6$-$(PPh_3)_3$ [c] | 2029 vs, 2006 m, 1998 s, 1954 m |
| $H_3Ru_3(CNEtBz)(CO)_6$-$(PPh_3)_3]^+$ [c] | 2055 m, 2036 vs, 1991 s |

[a] In dichloromethane.
[b] In hexanes.
[c] In $CDCl_3$.

Table 2
$^1$H NMR data in $CDCl_3$ solution

| Cluster | $^1$H NMR (ppm), $J$ (Hz) |
|---|---|
| $H_3Ru_3(CSEt)(CO)_6(PPh_3)(dppm)$ | −17.54(t, 1H, $J_{PH} = 14.6$)<br>−16.06(m, 2H, $J_{PH} = 10.0$)<br>1.34(t, 3H, $J_{HH} = 7.2$)<br>2.90(q, 2H, $J_{HH} = 7.2$)<br>3.48(d, 1H, $J_{HH} = 4.8$)<br>5.79(dt, 1H, $J_{HH} = 48$, $J_{PH} = 12.4$) |
| $H_3Ru_3(CSEt)(CO)_7(dppm)$ | −17.68(t, 1H, $J_{PH} = 14.2$)<br>−16.61(dt, 2H, $J_{HH} = 2.4$, $J_{PH} = 18.0$)<br>1.34(t, 3H, $J_{HH} = 7.6$)<br>2.80(q, 2H, $J_{HH} = 7.5$)<br>2.93(dt, 1H, $J_{HH} = 48$, $J_{PH} = 11.6$)<br>5.70(dt, 1H, $J_{PH} = 12.4$) |
| $H_3Ru_3(COMe)(CO)_6(PPh_3)$-(dppm) | −17.62(t, 1H, $J_{PH} = 13.6$)<br>−15.88(m, 2H)<br>3.05(m, 2H, $J_{PH} = 11.2$)<br>3.76(s, 3H)<br>4.39(m, 1H, $J_{PH} = 12.4$) |
| $H_3Ru_3(COMe)(CO)_7(dppm)$ | −17.82(t, 1H, $J_{PH} = 13.6$)<br>−16.40(m, 2H)<br>3.09(m, 2H, $J_{PH} = 11.5$)<br>3.69(s, 3H)<br>4.35(m, 1H, $J_{HH} = 5.4$, $J_{PH} = 12.3$) |
| $H_3Ru_3(CNMeBz)(CO)_7(PPh_3)_2$ | −16.28 (dd, 2H, $J_{HH} = 2.4$, $J_{PH} = 8.4$)<br>−15.74 (tt, 1H, $J_{HH} = 2.8$, $J_{PH} = 9.0$)<br>2.91(s, 3H)<br>4.43(s, 2H) |
| $H_3Ru_3(CNMeBz)(CO)_6(PPh_3)_2$-(ax-CNBz) | −16.01(d, 2H, $J_{PH} = 8.4$)<br>−15.55(t, 1H, $J_{PH} = 9.4$)<br>2.89(s, 3H)<br>4.43(s, 2H)<br>4.47(s, 2H) |
| $H_3Ru_3(CNMeBz)(CO)_6(PPh_3)_2$-(eq-CNBz) | −16.87(d, 1H, $J_{PH} = 10.0$)<br>−16.44(d, 1H, $J_{PH} = 10.4$)<br>2.86(s, 3H)<br>4.27(d, 1H, $J = 14.0$)<br>4.57(d, 1H, $J = 14.0$)<br>4.67(m, 2H) |
| $H_3Ru_3(CNEtBz)(CO)_7(PPh_3)_2$ | −16.19(dd, 2H, $J_{HH} = 2.4$ $J_{PH} = 8.0$)<br>−15.72(tt, 1H, $J_{HH} = 2.8$ $J_{PH} = 9.0$)<br>1.04(t, 3H, $J = 7.0$)<br>3.54(q, 2H, $J = 7.2$)<br>4.64(s, 2H) |
| $H_3Ru_3(CNEtBz)(CO)_6(PPh_3)_3$ | −15.06(br, 3H)<br>0.94(t, 3H)<br>3.5(br, 2H)<br>4.8(br, 2H) |

Phenyl resonances are not reported.

### 2.2. Electrochemistry

Electrochemical experiments were performed with the BAS-100B electrochemical analyzer using BAS-100W version 2.0 software. All measurements were made via

standard techniques. Solutions were purged with nitrogen and the atmosphere was maintained by a solvent saturated nitrogen blanket over the analyte mixture in the electrochemical cell. Solvents (dichloromethane and/or acetonitrile) were freshly distilled from calcium hydride and stored under nitrogen. The supporting electrolyte was tetrabutylammonium tetrafluoroborate (TBATFB). The working electrodes were platinum disk electrodes of 1.6 mm and 100 μm diameters, with electrolyte concentrations of 100 and $\geq 50$ mM, respectively. A silver wire served as the auxiliary (counter) electrode. The concentration of analyte was 1.0 mM, unless stated otherwise. The Ag | AgCl reference and the Ag wire quasi reference electrodes were employed. However, all potentials have been referenced to the ferrocene/ferrocenium couple. The latter was obtained experimentally by adding ferrocene as an internal standard. The peak-to-peak separation for ferrocene, $\Delta E_p = E_{pa} - E_{pc}$, was $65 \pm 5$ mV (1.6-mm diameter Pt electrode) and $73 \pm 7$ mV (100-μm diameter Pt electrode). Compensation for resistive losses ('iR drop') was used for all measurements allowed by the software. Digital simulations were performed using BAS DIGISIM version 2.1 software.

### 2.3. Kinetics by EPR spectroscopy

The decomposition of the 47-e clusters was monitored by loss of the EPR signal. EPR spectra were recorded on an IBM/Bruker X-band ER-200 SRC spectrometer, with a Bruker ER 035M gaussmeter, and Hewlett Packard 5350B frequency counter. In a typical reaction, about 0.006 mmol of the 48-e cluster was dissolved in 300 μl of dichloromethane in a custom glassware mixing apparatus with two side arms and a Schlenk connection. One side arm was a 4-mm glass EPR tube and the other was used as a chemical addition port. The solution was cooled to approximately 200 K in an acetone/dry ice bath. The 47-e cluster was generated by addition of a ferrocinium tetrafluoroborate (FcTFB) solution of known concentration in dichloromethane. If additional reagents were used, they were added subsequent to the oxidation step. The solution was mixed well, poured into the EPR tube side arm, and allowed to equilibrate to the desired temperature in the EPR cavity. The instrument was tuned and a series of EPR spectra were recorded. Intensity versus time plots were fit to a second-order equation yielding $k_{obs}$ as the slope and assuming quantitative initial formation of the 1-e oxidation product.

### 2.4. Fenske–Hall calculations

Standard Fenske–Hall calculations [13] were performed on $H_3Ru_3(CX)(CO)_9$, X = OH, Me, Cl and $NH_2$, and $H_3Ru_3(COH)(CO)_{9-n}(PH_3)_n$. Version 5.1 of the program (1989, provided by M.B. Hall) was used, employing Herman–Skilman basis functions. The FORTRAN code was compiled and run on a PC. Separate programs were written to analyze the data. These include a routine to draw contour maps of the orbitals. This program used a simple Slater orbital basis set.

The calculated HOMO energies are consistent with the observed electrochemical oxidation potentials (and the conventional understanding of substituent effects) for all of the clusters, with the exception of $H_3Ru_3(CCl)(CO)_9$. In order to test the reliability of the Fenske–Hall algorithm, we ran the routine for analogous substituted benzenes $XC_6H_5$. The calculated HOMO energies correlate with the trend in gas-phase ionization energies [24], except for chlorobenzene (X = H, −14.28 eV; Me, −13.62 eV; OH, −11.89 eV; $NH_2$, −10.60 eV; Cl, −11.59 eV). In an attempt to improve the data we used a larger basis set for the chlorine atom, including 3d orbitals. This made no qualitative difference and only a small quantitative difference. We conclude that the Fenske–Hall calculation does not correctly represent the sigma withdrawing versus the π donating character of the halogens. In what follows, therefore, the calculated results for $H_3Ru_3(CCl)(CO)_9$ cannot be considered reliable. For all other species, the calculated results are qualitatively in agreement with either expectation or experiment.

## 3. Results and discussion

The objective of this study is to delineate the mechanism of decomposition of the 47-e clusters $[H_3Ru_3(CX)(CO)_{9-n}L_n]^+$. To accomplish this objective, we first wanted to understand the basis for the ligand additivity relationship which defines the oxidation potential of the 48-e/47-e redox couple as a function of the substituent X and the identity of L and the degree of substitution $n$. Since the decomposition will be shown to occur by disproportionation, we also wanted to assess the properties of the 46-e clusters $[H_3Ru_3(CX)(CO)_{9-n}L_n]^{2+}$, which can be generated electrochemically, but are too unstable to be characterized by other methods. In the absence of significant structural rearrangement the ligand additivity relationship for the 46-e/47-e couple should be similar to that for the 47-e/48-e couple. Finally we wanted to determine the kinetics and mechanism for decomposition of $[H_3Ru_3(COMe)(CO)_6(PPh_3)_3]^+$, which is stable enough to allow spectroscopic characterization and also which is the only decomposition for which the products are fully characterized.

### 3.1. Review of prior work

The 48-e clusters $H_3Ru_3(\mu_3\text{-}CX)(CO)_{9-n}L_n$ have provided a wealth of information about the reactivity of small metal clusters. The substitutional behavior has been explored and structural features established [11]. The crystal structure of $H_3Ru_3(CPh)(CO)_7(AsPh_3)_2$ [11] showed both $AsPh_3$ ligands in axial sites, *trans* to the Ru–CPh bond, whereas $H_3Ru_3(COMe)(CO)_7$-$\{(PPh_2)_2CHPPh_2\}$[5] contains equatorially coordinated phosphorus donors because of ring strain which prevents diaxial coordination. Two isomers were found for $H_3Ru_3(\mu_3\text{-}CX)(CO)_6(PPh_3)_2L$ [6]. Generally, smaller L, e.g. CNBz, prefer equatorial sites, while larger ligands, e.g. $PPh_3$, occupy axial sites in the 48-e clusters.

The electrochemical and chemical 1-e oxidations of $H_3Ru_3(\mu_3\text{-}CX)(CO)_{9-n}L_n$ were studied previously [6,20]. The square scheme in Fig. 1 describes the process for $H_3Ru_3(COMe)(CO)_6(PPh_3)_3$. The equilibrium ratio $H_3Ru_3(\mu_3\text{-}COMe)(CO)_6(ax\text{-}PPh_3)_2(eq\text{-}PPh_3)/H_3Ru_3(\mu_3\text{-}COMe)(CO)_6(ax\text{-}PPh_3)_3$ was determined to be 0.15 at room temperature in dichloromethane, but EPR spectroscopy shows that the 47-e cation exists primarily as $[H_3Ru_3(\mu_3\text{-}COMe)(CO)_6(ax\text{-}PPh_3)_2(eq\text{-}PPh_3)]^{1+}$. Digital simulations of the cyclic voltammograms were used to determine rate constants and equilibrium constants, shown in Fig. 1 [6].

The 48-e/47-e oxidation potentials for a variety of clusters $H_3Ru_3(\mu_3\text{-}CX)(CO)_{9-n}L_n$ have been analyzed as an example of ligand additivity in a metal cluster system [6]. Lever's ligand parameters [14] were used to show that the 1-e oxidation potentials displayed ligand additivity according to Eq. (1):

$$E_{obs}\ (V) = S_{M3}\Sigma E_L(L_i) + 2.303(RT/nF)\rho\sigma_p^+(X) + I_{M3} \quad (1)$$

Eq. (1) is a modified version of Lever's with inclusion of a Hammett term for the methylidyne substituent [15]. Here the ligand parameters $E_L$ are summed over the nine CO or $ER_3$ ligands of the triruthenium core and the substituent parameters are summed over the $n$ hydrocarbyl substituents $X_i$, in this case the single methylidyne substituent. The coefficient $\rho$ represents the sensitivity of the oxidation potential to the electronic properties of the methylidyne substituent. The experimental value of 6.0(0.7) is consistent with the strong π donor interaction involving the methylidyne substituent.

The first term in Eq. (1) represents the effect of ligand substitution for CO upon the oxidation potential of the cluster. The linearity of the fit, which includes clusters differing in the number of metal atoms which are substituted, is consistent with equal contributions by each metal atom to the HOMO. As for monometallic complexes, ligand additivity is conserved [16]. The value of $S_{M3} = 0.37(0.03)$, compared with the value of 1 expected for a monometallic Ru complex, indicates that delocalization over the three Ru atoms reduces the dependence of the oxidation potential upon a ligand on any given Ru atom. Substitution of each phosphine for a carbonyl decreases the oxidation potential by 150–200 mV per ligand. There appears to be only a small dependence of oxidation potential upon the geometry of the substitution product. The oxidation potential for $H_3Ru_3(COMe)(CO)_6(ax\text{-}PPh_3)_2(eq\text{-}PPh_3)$ is 95 mV less positive than that of $H_3Ru_3(COMe)(CO)_6(ax\text{-}PPh_3)_3$.

The 47-e clusters were found to decompose over a period of minutes to hours. For one system, $[H_3Ru_3(\mu_3\text{-}COMe)(CO)_6(ax\text{-}PPh_3)_2(eq\text{-}PPh_3)]^{1+}$, the decomposition products were identified as 48-e $H_3Ru_3(\mu_3\text{-}COMe)(CO)_6(PPh_3)_3$, $[MePPh_3]^{1+}$, and the 46-e cluster $[H_3Ru_3(CO)_7(PPh_3)_3)]^{1+}$. The unusual stabilities of these 47-e clusters and the surprising 46-e decomposition product prompted us to study in more detail the mechanism of the decomposition reaction, the subject of this paper.

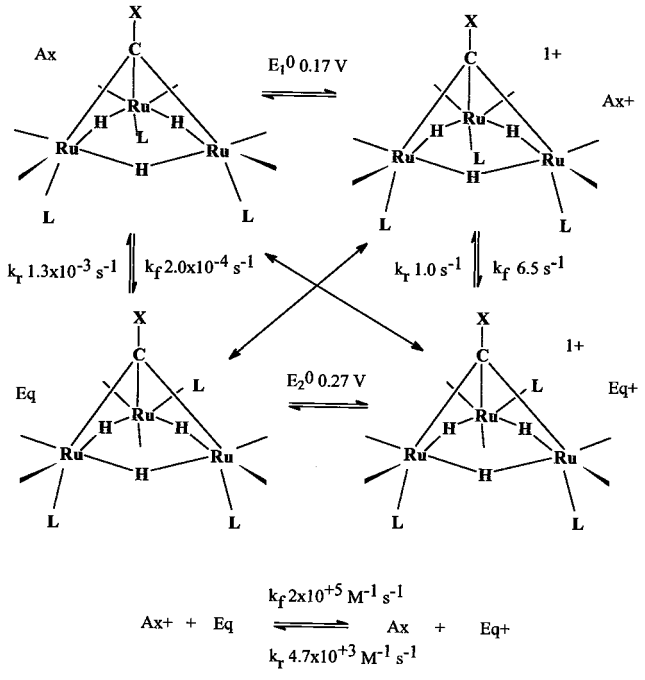


Fig. 1. Square scheme established previously for 48-e/47-e couple derived from $H_3Ru_3(COMe)(CO)_6(PPh_3)_3$.

### 3.2. 48-e Clusters

For the purposes of this study the substituted clusters $H_3Ru_3(\mu_3\text{-}CSEt)(CO)_7(dppm)$, $H_3Ru_3(\mu_3\text{-}CSEt)(CO)_6$-$(dppm)(PPh_3)$, $H_3Ru_3(\mu_3\text{-}COMe)(CO)_7(dppm)$, $H_3Ru_3$-$(\mu_3\text{-}COMe)(CO)_6(dppm)(PPh_3)$, $H_3Ru_3(\mu_3\text{-}CNMeBz)$-$(CO)_7(PPh_3)_2(CNBz)$, $H_3Ru_3(\mu_3\text{-}CNEtBz)(CO)_7(PPh_3)_2$, and $H_3Ru_3(\mu_3\text{-}CNEtBz)(CO)_6(PPh_3)_3$ were prepared by ligand substitution on the parent carbonyls. Spectroscopic data are analogous to other substituted alkylidy-

Table 3
EPR spectral data from dichloromethane solution, measured at ambient temperature unless noted

| Cluster | $g$ | $a$ (G) | $a$ (MHz) |
|---|---|---|---|
| $[H_3Ru_3(COMe)(CO)_8(PPh_3)]^+$ [a] | 2.081 (d) | 61.6 | 179.4 |
| $[H_3Ru_3(COMe)(CO)_7(PPh_3)_2]^+$ [a] | 2.082 (t) | 50.1 | 146.0 |
| $[H_3Ru_3(COMe)(CO)_6(PPh_3)$-(dppm)]$^+$ | 2.089 (d) | 32.3 | 94.49 |
| $[H_3Ru_3(CSEt)(CO)_7(PPh_3)_2]^+$ | 2.070 (t) | 46.4 | 134.6 |
| $[H_3Ru_3(CSEt)(CO)_7(dppm)]^+$ [b] | 2.072 (s) | | |
| $[H_3Ru_3(CNMeBz)(CO)_6(PPh_3)_2$-(CNBz)]$^+$ | 2.066 (t) | 50.8 | 147.0 |

[a] Measured at 260 K.
[b] Measured at 240 K.

nes characterized previously [5,6,11,20]. Dppm in each case occupies equatorial (eq) sites, *cis* to the Ru–CX bonds, on two different Ru atoms, as found for $H_3Ru_3(\mu_3\text{-}COMe)(CO)_7\{(PPh_2)_2CHPPh_2\}$ [5]. All $PPh_3$ ligands occupy axial (ax) sites *trans* to the Ru–CX bonds. The $H_3Ru_3(\mu_3\text{-}CNMeBz)(CO)_6(ax\text{-}PPh_3)_2(eq\text{-}CNBz)/H_3Ru_3(\mu_3\text{-}CNMeBz)(CO)_6(ax\text{-}PPh_3)_2(ax\text{-}CNBz)$ ratio in deuteriochloroform is 6.8 at room temperature.

### 3.3. 47-e Clusters

Chemical or electrochemical oxidations of the 48-e clusters generate 47-e cluster cations $[H_3Ru_3(CX)(CO)_{9-n}L_n]^{1+}$, analogous to those previously reported [6]. EPR spectral data (Table 3) were used to characterize the more stable of these. By the criteria that axially coordinated phosphines display hyperfine coupling of ca. 40–60 G and no resolvable coupling is observed for equatorial phosphines, the structures of the 47-e cations can be inferred. $[H_3Ru_3(COMe)(CO)_8(ax\text{-}PPh_3)]^{1+}$ and $[H_3Ru_3(COMe)(CO)_7(ax\text{-}PPh_3)_2]^{1+}$ contain axially coordinated phosphine ligands. Dppm ligands are equatorially coordinated ($[H_3Ru_3(COMe)(CO)_7$-(eq,eq-dppm)]$^{1+}$, $[H_3Ru_3(CSEt)(CO)_7(eq,eq\text{-}dppm)]^{1+}$, and $[H_3Ru_3(COMe)(CO)_7(eq,eq\text{-}dppm)(ax\text{-}PPh_3)]^{1+}$), whereas the $PPh_3$ ligand is axial. The EPR spectrum of $[H_3Ru_3(CMeBz)(CO)_7(PPh_3)_2(CNBz)]^{1+}$ displays a triplet, indicating axial $PPh_3$ ligands, but this cannot be distinguished from a dd pattern with coincidentally identical $^{31}P$ hyperfine couplings, so the coordination of the CNBz ligand is not established, although equatorial coordination is likely. The EPR data establish that the square scheme analogous to that shown in Fig. 1 is appropriate only for $H_3Ru_3(COMe)(CO)_6(ax\text{-}PPh_3)_3$ and $H_3Ru_3(CSEt)(CO)_6(ax\text{-}PPh_3)_3$, whereas axial–equatorial rearrangements are not involved in the electrochemistry for $H_3Ru_3(CX)(CO)_6(ax\text{-}PPh_3)_3$, X = Ph, NRR′, $H_3Ru_3(COMe)(CO)_6(eq\text{-}dppm)(PPh_3)$, or $H_3Ru_3(COMe)(CO)_{9-n}(ax\text{-}PPh_3)_n$, $n = 1$ or 2.

Electrochemical data for the 48-e/47-e couples are given in Table 4. As found previously the oxidation potential decreases as the degree of phosphine substitution increases. Di-equatorially coordinated dppm has about the same effect on the oxidation potential as di-axially coordinated $PPh_3$, suggesting little difference in oxidation potentials of isomers, but the 47-e products with dppm as a ligand are less stable than the $PPh_3$ analogs and the CVs display greater irreversibility.

### 3.4. Molecular orbital analysis

The bonding of $(\mu\text{-}H)_3Ru_3(\mu_3\text{-}CX)(CO)_9$, X = H, Cl, and Br, has been the subject of a previous study by

Table 4
Electrochemical data for $H_3Ru_3(CX)(CO)_{9-n}L_n$

| Cluster | $v$ (V s$^{-1}$) | $E_1^o$ (mV) | $\Delta E_{p1}$ (mV) | $i_{pc1}/i_{pa1}$ | $E_{pa2}$ (mV) | $E_2^o$ (mV) | $\Delta E_{p2}$ (mV) | $i_{pc2}/i_{pa2}$ |
|---|---|---|---|---|---|---|---|---|
| $H_3Ru_3(CSEt)(CO)_7(dppm)$ | 1.0 | 27 | 135 | 0.80 | 335 | Irreversible | | |
| $H_3Ru_3(CSEt)(CO)_6(PPh_3)_3$ | 0.1 | −185 | 86 | 0.83 | 280 | 231 | 98 | 0.35 |
| $H_3Ru_3(CSEt)(CO)_6(PPh_3)(dppm)$ | 1.0 | −173 | 106 | 0.79 | 110 | 47 | 127 | 0.44 |
| $H_3Ru_3(COMe)(CO)_7(dppm)$ | 1.0 | −6 | 126 | 0.49 | 210 | Irreversible | | |
| $H_3Ru_3(COMe)(CO)_6(PPh_3)dppm)$ | 0.1 | −175 | 91 | 0.46 | 220 | Irreversible | | |
| $H_3Ru_3(COMe)(CO)_9$ | 1.0 | [535] | ir | ir | Two-electron oxidation | | | |
| $H_3Ru_3(COMe)(CO)_9$ | 1.0 | 503[a] | 131 | 0.16 | Two-electron oxidation | | | |
| $H_3Ru_3(COMe)(CO)_8(PPh_3)$ | 1.0 | [282] | ir | ir | Two-electron oxidation | | | |
| $H_3Ru_3(COMe)(CO)_8(PPh_3)$ | 1.0 | 298[b] | 84 | 0.1 | 561 | Irreversible | | |
| $H_3Ru_3(COMe)(CO)_7(PPh_3)_2$ | 0.1 | 1 | 72 | 0.88 | 277 | 236 | 82 | 0.33 |
| $H_3Ru_3(COMe)(CO)_6(PPh_3)_3$ | 1.0 | −220 | 173 | 0.90 | 248 | 154 | 188 | 0.35 |
| $H_3Ru_3(CNMeBz)(CO)_6(SbPh_3)_3$ | 0.1 | −386 | 67 | 0.63 | 59 | Irreversible | | |
| $H_3Ru_3(CNMeBz)(CO)_7(PPh_3)_2$ | 1.0 | −425 | 80 | 0.95 | 36 | −18 | 109 | 0.52 |
| $H_3Ru_3(CNMeBz)(CO)_6(PPh_3)_3$ | 1.0 | −580 | 90 | 0.87 | −108 | −179 | 143 | 0.32 |
| $H_3Ru_3(CNEtBz)(CO)_6(PPh_3)_3$ | 0.1 | −626 | 70 | 0.73 | −125 | −200 | 150 | 0.40 |
| $H_3Ru_3(CNMeBz)(CO)_6(PPh_3)_2(CNBz)$ | 0.1 | −634 | 72 | 0.86 | −135 | −192 | 115 | 0.61 |
| $H_3Ru_3(COMe)(CO)_6(PPh_3)_2(P(OMe)_3)$ | 0.1 | −240 | 72 | 0.97 | 80 | | | |

Diffusion coefficients in dichloromethane: $H_3Ru_3(COMe)(CO)_7(PPh_3)_2$, $2.8(0.3)\times10^6$ cm$^2$ s$^{-1}$; $H_3Ru_3(CNMeBz)(CO)_7(PPh_3)_3$, $1.6(0.4)\times10^6$ cm$^2$ s$^{-1}$.
[a] At 250K
[b] At 200K

Table 5
Fenske–Hall calculations

| | SHOMO | HOMO | LUMO | Total Ru |
|---|---|---|---|---|
| Structure | | | | |
| $H_3Ru_3(CMe)(CO)_9$ | −8.4883 | −8.1885 | −0.0551 | 56.39 |
| $H_3Ru_3(CCl)(CO)_9$ | −7.9315 | −7.6861 | −0.9104 | 47.19 |
| $H_3Ru_3(COH)(CO)_9$ | −8.0845 | −7.2893 | −0.9972 | 48.7 |
| $H_3Ru_3(CNH_2\text{-}\parallel)(CO)_9$ | −8.2952 | −6.6664 | −0.411 | 43.55 |
| $H_3Ru_3(CNH_2\text{-}\perp)(CO)_9$ | −8.3209 | −6.5555 | −0.5626 | 44.38 |
| Phosphine compounds | | | | |
| $H_3Ru_3(COH)(CO)_8(ax\text{-}PH_3)$ | −7.5298 | −6.8262 | −0.7259 | 57.36 |
| $H_3Ru_3(COH)(CO)_8(eq\text{-}PH_3)$ | −7.4603 | −6.6212 | −0.2528 | 55.27 |
| $H_3Ru_3(COH)(CO)_7(PH_3)_2$ | −6.6159 | −6.0372 | 0.6548 | 61.86 |
| $H_3Ru_3(COH)(CO)_6(PH_3)_3$ | −5.9141 | −5.6009 | 0.9079 | 65.58 |

| | C-pz | C-px + py | R-pz | R-px + py |
|---|---|---|---|---|
| *Interior* | | | | |
| Structure | | | | |
| $H_3Ru_3(CMe)(CO)_9$ | 0 | 22.14 | 0 | −0.11 |
| $H_3Ru_3(CCl)(CO)_9$ | 15.16 | 5.57 | 10.99 | 4.26 |
| $H_3Ru_3(COH)(CO)_9$ | 3.31 | 15.64 | 3.24 | 11.93 |
| $H_3Ru_3(CNH_2\text{-}\parallel)(CO)_9$ | 14.89 | 0.03 | 26.06 | 0 |
| $H_3Ru_3(CNH_2\text{-}\perp)(CO)_9$ | 0.09 | 15.08 | 0 | 24.1 |
| Phosphine compounds | | | | |
| $H_3Ru_3(COH)(CO)_8(ax\text{-}PH_3)$ | 15.37 | 0.95 | 11.18 | 0.13 |
| $H_3Ru_3(COH)(CO)_8(eq\text{-}PH_3)$ | 6.59 | 10.53 | 3.5 | 8.76 |
| $H_3Ru_3(COH)(CO)_7(PH_3)_2$ | 9.01 | 5.94 | 3.67 | 5.5 |
| $H_3Ru_3(COH)(CO)_6(PH_3)_3$ | 10.05 | 4.72 | 3.12 | 4.46 |
| *Face* | | | | |
| Structure | | | | |
| $H_3Ru_3(CMe)(CO)_9$ | 16.88 | 5.25 | −0.09 | −0.03 |
| $H_3Ru_3(CCl)(CO)_9$ | 15.25 | 5.48 | 11.05 | 4.2 |
| $H_3Ru_3(COH)(CO)_9$ | 9.77 | 9.18 | 8.2 | 6.98 |
| $H_3Ru_3(CNH_2\text{-}\parallel)(CO)_9$ | 0.03 | 14.89 | 0 | 26.06 |
| $H_3Ru_3(CNH_2\text{-}\perp)(CO)_9$ | 11.41 | 3.78 | 17.75 | 6.34 |
| Phosphine compounds | | | | |
| $H_3Ru_3(COH)(CO)_8(ax\text{-}PH_3)$ | 11.36 | 4.95 | 7.39 | 3.92 |
| $H_3Ru_3(COH)(CO)_8(eq\text{-}PH_3)$ | 0.31 | 16.81 | 0.03 | 12.24 |
| $H_3Ru_3(COH)(CO)_7(PH_3)_2$ | 11.14 | 3.8 | 6.76 | 2.41 |
| $H_3Ru_3(COH)(CO)_6(PH_3)_3$ | 1.86 | 12.91 | 0.06 | 7.51 |

SHOMO, HOMO and LUMO columns contain the ionization energies of those orbitals in eV. The Total Ru column contains the percentage of the HOMO level on all three Ru atoms. The 'interior' plane is the plane that contains the apical carbon, the carbon substituent atom X and a Ru atom. The 'face' plane is the plane that contains the apical carbon and two Ru atoms. In both cases the $z$-axis is perpendicular to the plane. The $x$ and $y$ axes are oriented arbitrarily. C-pz is the percent HOMO in the apical carbon pz orbital. C-px + py is the sum of percentages in those apical carbon orbitals. R-pz is the population in the central atom of the X moiety, and likewise for the R-px + py column. For $H_3Ru_3(CNH_2)(CO)_9$ two different configurations were tested. For $H_3Ru_3(CNH_2\text{-}\parallel)(CO)_9$ the $NH_2$ plane lies in the molecular plane of symmetry, and for $H_3Ru_3(CNH_2\text{-}\perp)(CO)_9$, the $NH_2$ plane is perpendicular to the molecular plane of symmetry.

Sherwood and Hall [17]. Fenske–Hall MO calculations indicated that the HOMO for $H_3Ru_3(CX)(CO)_9$, X = H, Cl, Br, is involved primarily in the Ru–C bonding interaction. The methylidyne carbon was described as sp-hybridized with delocalized metal–carbon bonds, consisting of a weak bond involving the carbon 'lone pair', and a stronger interaction with the carbon 2p orbitals. The HOMO for X = H was described as Ru–C 'lone pair' antibonding. However, for X = Cl, Sherwood and Hall found that the interaction of the chlorine 3p electrons with the methylidyne carbon $2p_\pi$ orbitals pushes the 5e set to higher energy so that the HOMO is a degenerate pair. This set is overall Ru–C bonding. When the methylidyne substituent is a strong π donor group such as MeO, the electron pairs are strongly delocalized onto the cluster, thus accounting for the strong dependence of the oxidation potential upon the π donor properties of X.

To better assess the influence of $PR_3$ substitution and the methylidyne substituent, we conducted Fenske–Hall calculations for $H_3Ru_3(CX)(CO)_{9-n}(PR_3)_n$. For simplicity we generated coordinates for $H_3Ru_3(CX)(CO)_9$, X = OH, Me, Cl and $NH_2$, and $H_3Ru_3(COH)(CO)_{9-n}(PH_3)_n$, based upon previously reported crystallographic data for analogous compounds [5,11,18]. The purpose of our MO analysis was to better understand the electrochemistry of the cluster series. Toward this end we were primarily interested in the HOMO level, which is doubly degenerate for $C_{3v}$ symmetric methylidynes and non-degenerate otherwise. Unless otherwise stated, all data in this report concern the HOMO level only.

The basic data are given in Table 5. SHOMO, HOMO and LUMO columns contain the ionization energies of those orbitals in eV. The Total Ru column contains the percentage of the HOMO level on all three ruthenium atoms. The 'interior' plane is the same as in Sherwood and Hall: it is the plane that contains the apical carbon, the carbon substituent atom X and a Ru atom. The 'face' plane is the plane that contains the apical carbon and two Ru atoms. In both cases the $z$-axis is perpendicular to the plane. The $x$- and $y$-axes are oriented arbitrarily. The $H_3Ru_3(COH)(CO)_8(ax\text{-}PH_3)$ compound has a phosphine in the axial position, whereas $H_3Ru_3(COH)(CO)_8(eq\text{-}PH_3)$ has the phosphine in the equatorial position. For $H_3Ru_3(COH)(CO)_7(PH_3)_2$ and $H_3Ru_3(COH)(CO)_6(PH_3)_3$ all phosphines are in the axial positions. The planes are described as above. C-pz is the percent HOMO in the apical carbon pz orbital. C-px + py is the sum of percentages in those apical carbon orbitals. R-pz is the population in the methylidyne substituent atom X, and likewise for the R-px + py column. Two different conformations were tested for $H_3Ru_3(CNH_2)(CO)_9$, one with the plane of the $NH_2$ group coincident with the molecular plane of symmetry and one with perpendicular planes, and while there is an obvious difference in the orbital populations, there is little difference in the HOMO energies. We conclude from these data that they are qualitatively identical.

The Fenske–Hall routine was run for every configuration of the molecule, i.e. if the molecule was rotated the data was recalculated. Since it is an iterative, self-consistent algorithm, one expects small differences in the results. The differences were always less than 0.005 eV. Likewise, the total electron densities must be the same independent of whether or not the face or interior plane is considered. Thus, for example, if one compares the sum of the C-pz and C-px + py data for the interior plane, the value is equal that given for the face plane within the computational error. Likewise, the sum of R-pz and R-px + py are equal between the interior and face planes, to within the computational error.

The order of the HOMO levels corresponds to experiment, except for X = Cl as mentioned above. Consider first the interior plane. As shown in Table 5, the methyl group has no π bonding capability, and thus there is no HOMO electron density in the R–p orbitals. Chlorine, on the other hand, has orbitals available for π bonding, and thus contains significant population, as do the OH and $NH_2$ moieties. As expected, the $NH_2$ orbital population depends strongly on the orientation of the amine, as indicated by the difference between $H_3Ru_3(CNH_2\text{-}\|)(CO)_9$, in which the $NH_2$ plane lies in the molecular plane of symmetry, and $H_3Ru_3(CNH_2\text{-}\perp)(CO)_9$, in which the $NH_2$ plane is perpendicular to the molecular plane of symmetry.

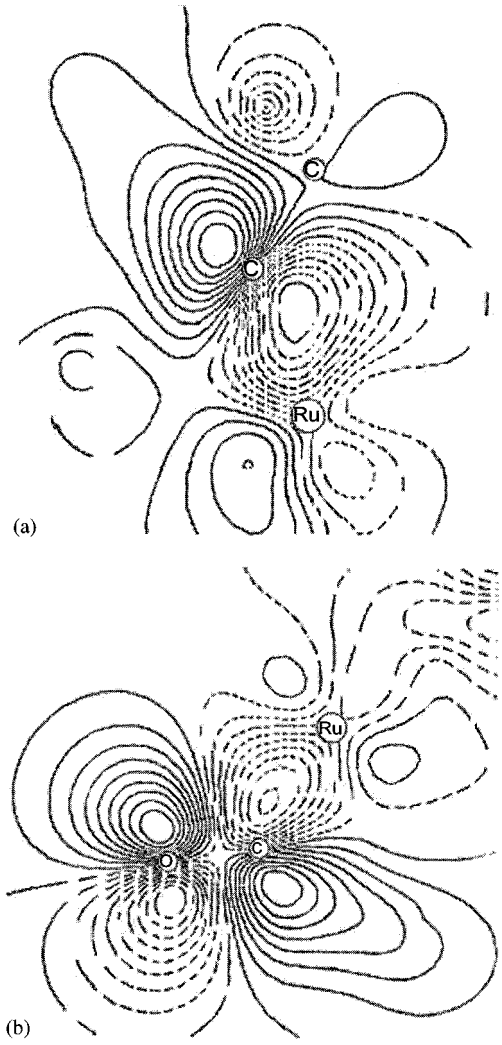


Fig. 2. Electron density contour maps for the interior plane for (a) $H_3Ru_3(CMe)(CO)_9$ and (b) $H_3Ru_3(COH)(CO)_9$. The carbon closest to the Ru atom is the methylidyne carbon and the other atom is the methylidyne substituent atom. Note the π antibond between C and O in (b).

The relevant π bond turns out in all cases to be anti-bonding, and thus has the effect of destabilizing the compound. This is seen for the chloro compound, though as stated the Fenske–Hall results in this case are unreliable. For the hydroxy and amino compounds the effect is more pronounced. This is illustrated in Fig. 2, which compares the methyl and hydroxy clusters, showing no π bonding in the former, and extensive π antibonding in the latter. This increasing anti-bonding tendency accounts for the lowered stability of the HOMO level and the lower oxidation potential found in the electrochemical experiments.

The other trend is the decrease in the electron density around the ruthenium centers. This trend roughly follows the electrochemical trend (the Cl moiety being a probably irrelevant exception). We find that much of the HOMO orbital is involved in the C–Ru bonds. As electron density is drawn into the C–X π antibond, density is correspondingly lowered in the C–Ru bonds. This is illustrated in the supplementary material, again comparing the Face projections for $H_3Ru_3(CX)(CO)_9$, X = OH and Me.

We now consider the effect of phosphine substitution for $H_3Ru_3(COH)(CO)_{9-n}(PH_3)_n$, where $n = 1$, 2 or 3. For $H_3Ru_3(COH)(CO)_8(PH_3)$, two cases were considered — the phosphine in an equatorial position (denoted $H_3Ru_3(COH)(CO)_8(\text{eq-}PH_3)$), or in an axial position (denoted $H_3Ru_3(COH)(CO)_8(\text{ax-}PH_3)$). In the other cases the phosphines were in the axial position.

Sequential substitution of π acid CO ligands by σ donor phosphine ligands causes a linear increase in the HOMO energy and also in the percent character of the HOMO on the Ru centers. The calculations reveal a slightly more positive oxidation potential for $H_3Ru_3(COH)(CO)_8(\text{ax-}PH_3)$ than for $H_3Ru_3(COH)(CO)_8(\text{eq-}PH_3)$. This result is consistent with the experimental data for $H_3Ru_3(COMe)(CO)_6(\text{ax-}PPh_3)_2(\text{eq-}PPh_3)$ and $H_3Ru_3(COMe)(CO)_6(\text{ax-}PPh_3)_3$. However, it is counter intuitive since one would expect greater electron donation from the axial phosphine than from the equatorial one (consistent with the larger axial hyper-fine coupling constant in the EPR spectra of the 47-e clusters), and hence the trend should be reversed.

The Fenske–Hall calculations show a probable reason for this effect. The phosphine ligands contribute insignificantly to the HOMO level, and hence any σ-

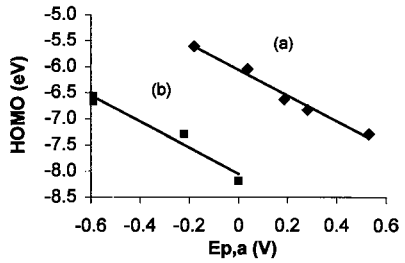


Fig. 3. Correlation of calculated HOMO energy for (a) $H_3Ru_3(COH)(CO)_{9-n}(PH_3)_n$ versus anodic peak potential $E_{p,a1}$ for the $H_3Ru_3(COMe)(CO)_{9-n}(PPh_3)_n$ and (b) $H_3Ru_3(CX)(CO)_9$, X = Me, OH, $NH_2$, versus anodic peak potential $E_{p,a1}$ for the $H_3Ru_3(CX)(CO)_6(PPh_3)_3$, X = Me, OMe, NMeBz.

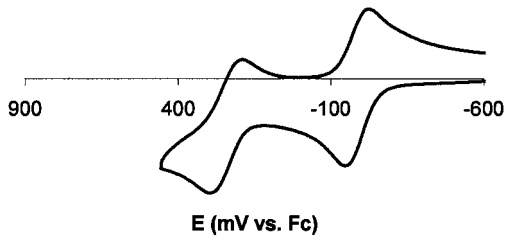


Fig. 4. CV of $H_3Ru_3(CSEt)(CO)_6(PPh_3)_3$ at 2 V $s^{-1}$.

bonding effects do not show up there. On the other hand, π interactions with the equatorial carbonyls, but not the axial carbonyls, do lower the energy of the HOMO level. Thus, the observed effect is due to the orientation of the carbonyl, rather than the phosphine directly.

The expected trend is seen with the addition of multiple phosphines, all to the axial position. The HOMO density in the Ru centers increases with each phosphine addition. This reflects the σ-donor properties of the phosphine ligand. The metal center density is lower for the phosphine in the equatorial position, consistent with the expectation that equatorial phosphines will be better donors than axial ones.

Apart from R = Cl, the excellent correlation between the calculated HOMO energies and the electrochemical oxidation potentials (Fig. 3) gives us confidence that we can account for the ligand additivity relationship found experimentally for the 1-e oxidations. The linear relationship between HOMO energies and electrochemical oxidation potentials has been noted many times for monometallic complexes [16]. In the absence of significant structural differences between 48-e, 47-e and 46-e clusters of a related series, the ligand additivity relation for the 47-e/46-e redox couple should be similar to that for the 48-e/47-e redox couple.

### 3.5. Second 1-e oxidation

As will be demonstrated below, the apparent mechanism for decomposition of the 47-e clusters is disproportionation to generate 48-e and 46-e clusters. The 46-e products are too unstable to characterize spectroscopically, but they can be studied by electrochemical methods. In our previous study of this system using cyclic voltammetry, we noted that the second 1-e oxidations for $H_3Ru_3(COMe)(CO)_{9-n}(PPh_3)_n$, $n = 2$ and 3, were irreversible and no other cathodic waves were seen on the reverse scans, while for $n = 0$ and 1, only a single anodic wave was observed. In this work we have examined the 2-e oxidations in more detail, especially as they pertain to the decomposition of the 47-e clusters.

Throughout the following discussion, it must be noted that the peak potentials of irreversible and quasi-reversible electrochemical processes are affected by the kinetics and in a highly resistive solvent such as dichloromethane these potentials are also affected by uncompensated solution resistance. Consequently quantitative thermodynamic conclusions from these should be viewed with caution.

The CV of $H_3Ru_3(CSEt)(CO)_6(PPh_3)_3$ displays a nearly reversible 1-e oxidation at $-0.185$ V and a nearly irreversible 1-e oxidation at $E_{p,a2}$ $+0.280$ V at 100 mV $s^{-1}$. As the scan rate ($v$) increases from 50 mV $s^{-1}$ to 5 V $s^{-1}$ the current ratio increases for both the first and second oxidations, consistent with an EC description for both. At 2 V $s^{-1}$ (Fig. 4) both 1-e oxidations are electrochemically reversible. Digital simulations were used to estimate the life-time for the 46-e product of the second oxidation, assuming a first-order decomposition, as ca. $2 \times 10^{-2}$ s. This compares with the half-life of $2 \times 10^{+2}$ s for the 47-e species determined by EPR methods (below).

The CV of $H_3Ru_3(COMe)(CO)_6(PPh_3)_3$ was previously examined in detail [6]. As noted the second 1-e oxidation is irreversible at low scan rates. This process is quasi-reversible at scan rates above 1 V $s^{-1}$.

The CV of $H_3Ru_3(COMe)(CO)_7(PPh_3)_2$ in dichloromethane (Fig. 5(a)) also displays a nearly reversible 1-e oxidation followed by a nearly irreversible second 1-e oxidation. As noted previously, the second 1-e oxidation is irreversible at low scan rates. We find now that this process becomes quasi-reversible at scan rates above 1 V $s^{-1}$. We had previously observed that CVs were irreversible in acetonitrile. The effect of acetonitrile was investigated by conducting electrochemical experiments in various dichloromethane–acetonitrile mixtures. The effect of increased percentages of acetonitrile was: (a) to decrease the chemical reversibility of the first oxidation but without significantly affecting the oxidation potential, and (b) to shift the anodic peak of the second oxidation in a negative direction, closer to the first oxidation couple.

The cyclic voltammogram of $H_3Ru_3(COMe)(CO)_8(PPh_3)$ in dichloromethane displays an almost completely irreversible 2-e wave (based upon the anodic peak current and the estimated diffusion coefficient)

oxidation at low scan rates ($E_{p,a}$ 0.28 V), but becomes quasi-reversible at ca. 50 V $s^{-1}$. At scan rates of at least 1 V $s^{-1}$, upon continuing the cathodic sweep upon scan reversal, a cathodic peak appears at $-0.82$ V; this peak is not observed if the scan is initiated in the negative direction, so this new electroactive species is formed in response to the oxidation. The peak separation $\Delta E_p$ for the anodic couple of 106 mV at 50 V $s^{-1}$ decreases to about 80 mV at 100 V $s^{-1}$, indicating that the quasi-reversibility is due to a follow-up chemical reaction rather than slow electron transfer. Therefore, a qualitative inspection indicates the electrochemistry of $H_3Ru_3(COMe)(CO)_8(PPh_3)$ exhibits an EC mechanism. Low temperature CVs ($\sim$200 K) show two broad anodic peaks at 0.30 and 0.56 V, attributed to the 48/47-electron couple and the 47/46-electron couples, respectively.

In cases where the coupled chemical process is a fast second-order reaction, such as disproportionation or dimerization, the initial redox peak ($E_p$) shifts (anodically for an oxidation) 20 mV/n for each 10-fold increase in scan rate. On the contrary, a first-order process should display a 30/n mV shift in $E_p$ for each 10-fold increase in scan rate. This guideline, based on Eq. (2), permits one to evaluate the slope of an $E_p$ versus log $v$ plot for compliance.

$$E_p = E_{\frac{1}{2}} - 0.902(RT/nF) + (RT/3nF)\ln(2/3\lambda_2) \quad (2)$$

where $\lambda_2 = k_2 C_r RT/nFv$

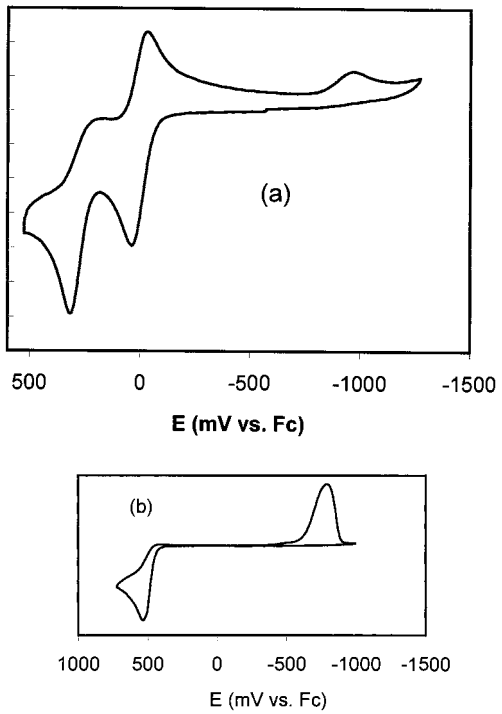


Fig. 5. CVs at 1 V $s^{-1}$ for (a) $H_3Ru_3(COMe)(CO)_7(PPh_3)_2$ and (b) $H_3Ru_3(COMe)(CO)_9$.

The plot of $E_{pa}$ for $H_3Ru_3(COMe)(CO)_8(PPh_3)$ versus log $v$ yields a slope of 20.1(1.5) mV, indicating a second-order decomposition for the 1-e oxidation product. This suggests that the electrochemistry involves a 1-electron oxidation followed by a rapid second-order disproportionation (Eqs. (3) and (4)), resulting in an EC mechanism. The mechanism cycles back to Eq. (3) until 2 mol of electrons have been consumed per mol of 48-electron complex. Since the value of $E_{1/2}$ is not known, we cannot accurately determine the rate constant, but if the value is taken as 0.21–0.23 V, then $k$ is between 150 and 1500 $M^{-1}$ $s^{-1}$. The addition of 20 equivalents of $PPh_3$ to a solution of 1.4 mM $H_3Ru_3(COMe)(CO)_8(PPh_3)$ in dichloromethane was accompanied by a ca. 50% decrease in the anodic peak current due to the 47-e/46-e couple, and a (ca 75%) decrease in the cathodic peak current of 47-e product, observed in the reverse cathodic scan; this result is consistent with an increase in the rate of decomposition of the 47-e cluster by a factor of ca. 2.

$$48e \rightarrow 47e + e- \qquad E \quad (3)$$

$$2\ 47e \rightarrow 48e + 46e \qquad C \quad (4)$$

$$46e \rightarrow \text{decomposition}$$

The CV of $H_3Ru_3(COMe)(CO)_9$ (Fig. 5(b)) at 1 V $s^{-1}$ displays an irreversible 2-e oxidation at $E_{p,a}$ 0.28 V; upon scan reversal, a new cathodic peak is observed at $-0.73$V, but only at high scan rates. Single scans of $H_3Ru_3(COMe)(CO)_9$ indicate very little diffusion of the dication away from the electrode, attributable to adsorption onto the surface. Multiple scans of $H_3Ru_3(COMe)(CO)_9$ were made by reversing the potential in the cathodic scans before and after reduction of the dication product, at both 1 and 50 V $s^{-1}$. A comparison of the anodic peak currents indicates significant current loss in the subsequent cycles when the scan is reversed before the cathodic wave, while very little current is lost when the cathodic scans proceed beyond the cathodic wave. Thus, the second 1-e oxidation is chemically but not electrochemically reversible at fast scan rates.

Similarly, CVs of $H_3Ru_3(COMe)(CO)_7(PPh_3)_2$, and $H_3Ru_3(COMe)(CO)_7(dppm)$ each display a cathodic peak at a potential considerably negative of the anodic peak for the second 1-e oxidation or 2-e oxidation. This new electroactive species is formed in response to the second ET, not the first. In the cases of $H_3Ru_3(COMe)(CO)_7(PPh_3)_2$, and $H_3Ru_3(COMe)(CO)_7$-(dppm) when the potential scan is reversed after the second oxidation wave, and scan rates are at least 1 V $s^{-1}$, reduction of the dication product is apparent at $-966$ and $-986$ mV, respectively. However, if the switching potential is just beyond the first oxidation (48/47-electron couple), these cathodic waves are not observed.

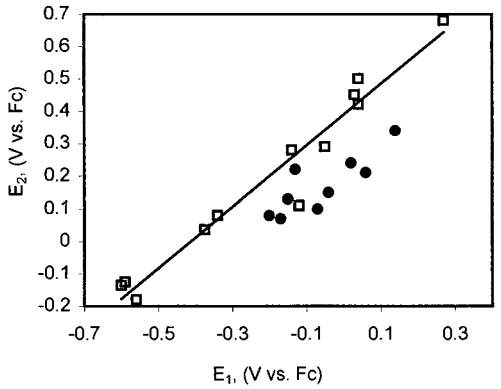


Fig. 6. Plot of anodic peak potentials for the second 1-e oxidations ($E_{p,a2}$) versus anodic peak potentials for the first 1-e oxidations ($E_{p,a1}$) for $H_3Ru_3(CX)(CO)_{9-n}L_n$. The squares are for X = Br, SEt, Me, Et, Ph, NMeBz, or NEtBz (the line is the least-squares fit for these values, $E_{p,a2} = 0.94E_{p,a1} + 0.39$), and the circles are X = OMe.

The observed electrochemistry is described by a square scheme as follows:

1. Electrochemical two-electron oxidation of $H_3Ru_3(COMe)(CO)_{9-n}(PPh_3)_n$.
2. Chemical conversion of $[H_3Ru_3(COMe)(CO)_{9-n}(PPh_3)_n]^{2+}$ to a new species, possibly an isomer, designated $*[H_3Ru_3(COMe)(CO)_{9-n}(PPh_3)_n]^{2+}$.
3. Two-electron reduction of $*[H_3Ru_3(COMe)(CO)_{9-n}(PPh_3)_n]^{2+}$ to its neutral form $*H_3Ru_3(COMe)(CO)_{9-n}(PPh_3)_n$.
4. Chemical conversion of $*H_3Ru_3(COMe)(CO)_{9-n}(PPh_3)_n$ back to $H_3Ru_3(COMe)(CO)_{9-n}(PPh_3)_n$.

Although the second 1-e oxidations are irreversible, the anodic peak potentials provide an estimate of the relative oxidation potentials. The second 1-e oxidation waves for $H_3Ru_3(COMe)(CO)_6(PPh_3)_3$ and $H_3Ru_3(COMe)(CO)_7(PPh_3)_2$ have $E_{p,a}$ of 0.25 (1.0 V $s^{-1}$) and 0.28 (0.1 V $s^{-1}$) V, respectively. The CV of $H_3Ru_3(COMe)(CO)_8(PPh_3)$ displays a single irreversible 2-e anodic wave at $E_{p,a}$ 0.28 V (1.0 V $s^{-1}$) at room temperature, but at 200 K two irreversible 1-e waves are seen ($E_{p,a}$ 0.29 and 0.56 V). For $H_3Ru_3(COMe)(CO)_9$ only a single, irreversible 2-e oxidation is observed at $E_{p,a}$ + 0.54 V (at 1.0 V $s^{-1}$). Fig. 6 shows a plot of the observed $E_{p,a1}$ for the first oxidation versus the observed $E_{p,a2}$ for the second oxidations for $H_3Ru_3(CX)(CO)_{9-n}(L)_n$, where determinable. Excellent linearity is displayed for X = Br, SEt, Me, Ph, Et, and NMeBz (square entries), however the values for X = OMe (circles) form a roughly parallel grouping ca. 100–200 mV below that for the others, indicating a less positive second oxidation potential, compared to the first. The linearity of the fit for X = Br, SEt, Me, Ph, Et, and NMeBz includes the most electrochemically reversible system ($H_3Ru_3(CSEt)(CO)_6(PPh_3)_3$), di- and trisubstituted clusters, the clusters with the most positive and least positive oxidation potentials, and couples involving axial–equatorial ligand migration; in fact, only $H_3Ru_3(CSEt)(CO)_6(dppm)(PPh_3)$ lies significantly off the best-fit line. On the other hand, the only member of the X = OMe series which is close to the line is $H_3Ru_3(COMe)(CO)_6(dppm)(PPh_3)$. Since the second 1-e oxidations are generally irreversible, and so shifted anodically from the true oxidation potential, the values of $\Delta E = E_{p,a2} - E_{p,a1}$ are greater than the thermodynamic differences in oxidation potentials, but the comparative values for the series are most likely significant. The lower $\Delta E$ for the OMe series suggests some participation by the OMe substituent in stabilizing the 46-e product by incipient coordination. A similar stabilizing effect was proposed to account for labilization of $HRu_3(\mu\text{-}COMe)(CO)_{10}$ for CO dissociation, a process also generating a 46-e intermediate. The values of $E_{p,a2} - E_{p,a1}$ of 0.2–0.4 V can be taken as a rough estimate of the thermodynamics for disproportionation ($K_D \sim 10^{-4}$–$10^{-7}$). The very similar ligand additivity relationships for the 47-e/46-e couple (with the possible exception of the OMe clusters as suggested above) and the 48-e/47-e couple suggest similar ground state electronic structures for all three redox states. A comprehensive analysis of the anodic peak potentials of the second 1-e oxidations for all complexes, according to Eq. (1) gives $\rho$ as 8.4(0.8) and $S_{M3}$ as 0.19(0.09), but it should be noted that we have few examples of 47-e/46-e peak potentials for mono- or disubstituted clusters.

The observation of 2-e irreversible oxidations for $H_3Ru_3(COMe)(CO)_8(PPh_3)$ and $H_3Ru_3(COMe)(CO)_9$ is attributed to second-order disproportionation and subsequent oxidation of the 48-e disproportionation product at the electrode, giving an overall 2-e process. This thermodynamically unfavorable disproportionation is driven by rapid, irreversible rearrangement and then decomposition of the 46-e product. At 200 K, decomposition of the 46-e product derived from $H_3Ru_3(COMe)(CO)_8(PPh_3)$ is slow enough that the second 1-e oxidation can be observed, with $E_{p,a2} - E_{p,a1}$ of ca. 0.27 V, consistent with Fig. 6.

We can speculate upon the nature of the rearrangement of the 46-e dication observed for $(\mu\text{-}H)_3Ru_3(COMe)(CO)_9$ and $(\mu\text{-}H)_3Ru_3(COMe)(CO)_8(PPh_3)$. We have previously proposed that CO dissociation from the molecule $(\mu\text{-}H)Ru_3(\mu\text{-}COMe)(CO)_{10}$ generates a stabilized '46-e' species $(\mu\text{-}H)Ru_3(\mu_3\text{-}\eta^2\text{-}COMe)(CO)_9$, stabilized via electron donation from the C–OMe bond [21]. A similar structure $[(\mu\text{-}H)_3Ru_3(\mu_3\text{-}\eta^2\text{-}COMe)(CO)_9]^{2+}$ (Fig. 7) would account for the very negative reduction potential of the rearranged product. Another possibility is deprotonation of the dication, giving $[(\mu\text{-}H)_2Ru_3(\mu_3\text{-}\eta^2\text{-}COMe)(CO)_9]^{1+}$ or $[(\mu\text{-}H)Ru_3(\mu_3\text{-}\eta^2\text{-}COMe)(CO)_9]$. Deprotonation has been observed for hydride-containing radical cations [23] and certainly the dications should be much more acidic than the monocation or neutral species. In fact decomposi-

tion of 47-e $[H_3Ru_3(COMe)(CO)_7(PPh_3)_2]^{1+}$ generates a small amount of $[H_3Ru_3(COMe)(CO)_8(PPh_3)_2]^{1+}$, which may be formed by deprotonation of the 46-e dication and pick-up of CO. The chemical reversibility shown by the cycles is perhaps more consistent with the simple isomerism, and the adsorption or precipitation of the rearranged product on the electrode is more consistent with a doubly charged species than a singly charged or uncharged one.

The results of the electrochemical investigations of the 46-e oxidation products allow us to conclude the following: (1) Once formed, the 46-e clusters are very unstable, reacting to form a new electroactive species (reducible at very negative potentials compared with the initial 46-e species), which itself decomposes rapidly to electrochemically-inactive products. (2) The second oxidation potential displays the same ligand effects as the first oxidation process, but is much more sensitive to medium effects, e.g. solvent or added nucleophiles. (3) The electrochemistry of $H_3Ru_3(COMe)(CO)_8(PPh_3)$ is described as an EC process with a second-order

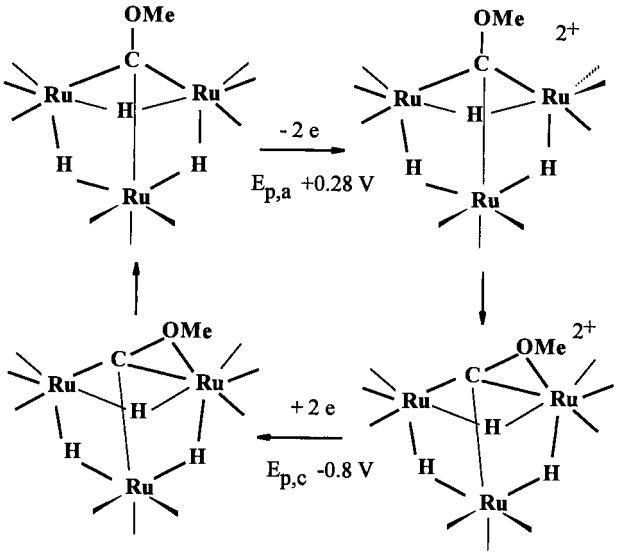


Fig. 7. Possible square scheme involving rearrangement of 46-e species.

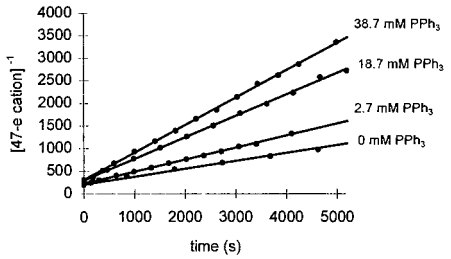


Fig. 8. Second-order plots of 1/[47-e] versus time, determined by decay of the EPR signal for $[H_3Ru_3(COMe)(CO)_6(PPh_3)_3]^{1+}$ at 294 K in dichloromethane in the presence of $PPh_3$ (0, 2.7, 18.7, and 38.7 mM).

disproportionation of the 47-e species ($k \sim 150$–$1500$ $M^{-1}$ $s^{-1}$).

### 3.6. Kinetics and mechanism of decomposition of 47-e $[H_3Ru_3(COMe)(CO)_6(PPh_3)_3]^{1+}$, $[H_3Ru_3(CSEt)(CO)_6(PPh_3)_3]^{1+}$, and $[H_3Ru_3(COMe)(CO)_7(PPh_3)_2]^{1+}$

The 47-e radicals $[H_3Ru_3(CX)(CO)_{9-n}L_n]^{1+}$, $n = 2$ or 3, decomposed over a period of minutes to hours, depending upon the substituent X and ligands L [6]. In all cases the corresponding 48-e cluster is formed in 40–60% yield, but generally no other products could be characterized. Decomposition of $[H_3Ru_3(COMe)(CO)_6(PPh_3)_3]^{1+}$ yielded 48-e products $H_3Ru_3(COMe)(CO)_6(PPh_3)_3$, $H_3Ru_3(COMe)(CO)_7(PPh_3)_2$, $H_3Ru_3(COMe)(CO)_8(PPh_3)$, $[H_2Ru_3(COMe)(CO)_7(PPh_3)_2]^{1+}$, and the 46-e cluster $[H_3Ru_3(CO)_7(PPh_3)_3]^{1+}$, in addition to some $MePPh_3^{1+}$, but mass balance is not achieved in the absence of added $PPh_3$. In the presence of one equivalent of added $PPh_3$ the stoichiometry is as shown in Eq. (5) [6]. The major focus of this work was on the mechanism of this decomposition reaction.

$$2\,[H_3Ru_3(COMe)(CO)_6(PPh_3)_3]^{1+} + PPh_3 \rightarrow [H_3Ru_3(CO)_7(PPh_3)_3]^{1+} + MePPh_3^{1+} + H_3Ru_3(COMe)(CO)_6(PPh_3)_3 \quad (5)$$

The progress of the decompositions of the 47-e clusters $[H_3Ru_3(COMe)(CO)_6(PPh_3)_3]^{1+}$, $[H_3Ru_3(CSEt)(CO)_6(PPh_3)_3]^{1+}$, and $[H_3Ru_3(COMe)(CO)_7(PPh_3)_2]^{1+}$ was monitored via the intensity of the EPR signal. The intensity versus time curves displayed excellent second-order fits, and poor first-order fits. Fig. 8 shows plots of $1/[[H_3Ru_3(COMe)(CO)_6(PPh_3)_3]^{1+}]$ versus time, in the presence and absence of added $PPh_3$. The linearity of the individual plots is typical for all of the compounds examined. Second-order rate constants $k_{obs}$ are given in the supplementary material. While the second-order rate constant for an individual experiment was well-determined by the data, reproducibility was difficult to achieve, requiring great care in sample preparation, and since the calculated rate constant is proportional to the initial concentration of 47-e cluster, it is sensitive to errors in weights of either cluster or oxidant, volume of solvent, and the presence of impurities which might cause some decomposition of the radical by other routes; consequently, the error limits are relatively poor, with reproducibility only within $\pm 25\%$ under the best conditions. Nonetheless, the general characteristics are reasonably well-behaved even though the products are unknown. The only system for which products were well-characterized and mass bal-ance was achieved was $[H_3Ru_3(COMe)(CO)_6(PPh_3)_3]^{1+}$, in the presence of added $PPh_3$, but it seems evident that the nature of the rate-determining step for decomposition of all of these is very similar.

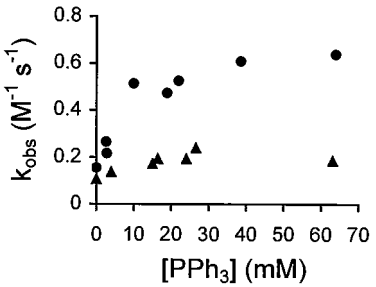


Fig. 9. Plots of the second-order $k_{obs}$ versus [$PPh_3$] for the decomposition of $[H_3Ru_3(COMe)(CO)_6(PPh_3)_3]^{1+}$ at 270 (triangles) and 294 K (circles).

We first examined the decomposition of $[H_3Ru_3(COMe)(CO)_6(PPh_3)_3]^{1+}$, in the presence of added $PPh_3$. The plot of $k_{obs}$ at 294 K versus [$PPh_3$] (Fig. 9) indicates acceleration of the rate by a factor of 2–3 by addition of 10 mM $PPh_3$, compared with decomposition in the absence of $PPh_3$, but after about 10 mM the rate constant increases only slightly with $PPh_3$ concentration.

Similar results were obtained at 270 K (Fig. 9). The higher rate of disproportionation in the presence of $PPh_3$ is difficult to explain fully. The phosphine dependence gives the appearance of a saturation behavior, with a two-term rate law, both terms second-order in 47-e cluster concentration and with comparable rate constants. However, the saturation is achieved at relatively low phosphine concentrations, ca. twice the initial concentration of $[H_3Ru_3(COMe)(CO)_6(PPh_3)_3]^{1+}$, yet the IR and EPR spectra of the 47-e cluster are unaffected by added phosphine. The effect of phosphine could also be attributed to a medium effect in which the local solvation environment facilitates electron transfer, but again the rapid change in rate constant at low [$PPh_3$] is unexpected. Kinetic data were more reproducible in the presence of $PPh_3$ so some of the difference may be due to experimental error. However, a possible explanation for the accelerating effect of $PPh_3$ at even low concentrations is a change in the stoichiometry of the decomposition. Fragmentation of the 46-e disproportionation product could generate mononuclear fragments which could act as either oxidants for the 48-e product or reductants for the 47-e clusters, thus changing the overall stoichiometry. One pertinent example of such a system is the electrolytic decomposition of $[Mo_2(CO)_{10}]^{2-}$, for which the number of electrons varies from 1.7 in dichloromethane in the presence of 10 equivalents of $PPh_3$ to 0.5 in its absence (corresponding to an apparent threefold change in rate), even though the mechanism appears to remain the same, namely EC second-order disproportionation [4]. Decomposition of the 46-e species in the absence of $PPh_3$ may produce fragments capable of oxidizing the 48-e product, thus reducing the apparent rate of disproportionation; consistent with this the isolated yield of 48-e cluster is less than 50% in most of these decompositions in the absence of $PPh_3$. Addition of $PPh_3$ scavenges the 46-e oxidation product by forming $[MePPh_3]^{1+}$ and 46-e $[H_3Ru_3(CO)_7(PPh_3)_3]^{1+}$. We believe that $PPh_3$ is not directly associated with the rate-determining step, except to the extent that its presence at high concentrations in solution affects the potential of the second 1-e oxidation, presumably by stabilizing the 46-e product (vide infra), in the same way that acetonitrile affects the potential and rate of decomposition.

The rate of this reaction is not significantly reduced by the addition of the 48-e cluster (also consistent with linear plots of 1/intensity to greater than 90% conversion). A CO atmosphere does not significantly affect the rate, although the large error limits make this difficult to say with certainty. Adding 0.1 M TBATFB increased the rate of decomposition by a factor of about two.

Addition of even a small amount of chloride (e.g. 4 mM) had a dramatic effect, decomposition being too fast to follow by EPR at 250 K. In this case the 48-e cluster is recovered in ca. 67% yield [6]. If a disproportionation reaction is assumed here too, then the 46-e product must decompose further in the presence of chloride to products capable of reducing the 47-e cluster, thus accounting for the greater than 50% yield of the 48e cluster. The effect of chloride is attributed to its ability to both form ion pairs and act as a nucleophile for the 46-e product. The importance of halide ion pairing in disproportionation of 17-e $[M(CO)_3(PCyc_3)_2]^{1+}$ has been demonstrated [19]. Uncharged nucleophiles $PPh_3$, NCMe, and pyridine and the non-nucleophilic salt TBATBF show much smaller rate accelerations.

The second-order dependence upon the 47-e cluster concentration rules out a mechanism involving rate-limiting nucleophilic attack by $PPh_3$. A second-order dependence could arise from rate-determining electron transfer, either before attack by $PPh_3$ on the 46-e dication or after reversible addition of $PPh_3$; however, the latter mechanism would give a first-order dependence on $PPh_3$ concentration, and while there is some acceleration of the rate by addition of $PPh_3$, the effect is quite small, even compared with the rate in the absence of any added nucleophile. Alternatively, second-order behavior could arise from a reversible disproportionation followed by a rate determining chemical reaction by the 46-e species thus formed; in this case saturation kinetics could account for the increase in rate in the presence of added $PPh_3$. Two observations are inconsistent with reversible disproportionation and rate-determining attack by $PPh_3$. First, the rate is independent of concentration of the 48-e species, shown by experiments in which 48-e precursor

was added to the solution and also by the excellent second-order plots even up to 90% conversion. Second, the electrochemical data allow us to estimate the equilibrium constants for disproportionation (Table 6) and also to assess the stability of the 46-e clusters formed in such a reaction. The irreversibility of the second 1-e oxidations in the CVs of $H_3Ru_3(COMe)(CO)_6(PPh_3)_3$, $H_3Ru_3(COMe)(CO)_7(PPh_3)_2$, $H_3Ru_3(CSEt)(CO)_6(PPh_3)_3$, and $H_3Ru_3(CNMeBz)(CO)_6(PPh_3)_3$ at lower scan rates shows that the 46-e clusters, once formed, decompose at rates much faster than decomposition of the 47-e clusters, so that the disproportionations cannot be chemically reversible. This then implies that the rate determining step involves the electron transfer itself:

$$2[H_3Ru_3(COMe)(CO)_6(L)_3]^{1+} \rightarrow H_3Ru_3(COMe)(CO)_6(L)_3 + [H_3Ru_3(COMe)(CO)_6(L)_3]^{2+} \quad \text{slow}$$

$$[H_3Ru_3(COMe)(CO)_6(L)_3]^{2+} + L \rightarrow [H_3Ru_3(CO)_7(L)_3]^{+} + MeL^{1+} \quad \text{fast}$$

The mechanism of outer-sphere electron transfer has been thoroughly studied (Ref. [1], pp. 6–26). The Marcus–Hush theory allows estimation of the rate constant for electron transfer as in Eq. (6):

$$k_{12} \sim (k_{11}k_{22}K_{12}f_{12})^{1/2} \text{ where } \ln f_{12} = (\ln K_{12})^2/4\ln(k_{11}k_{22}/Z^2) \quad (6)$$

Pertaining to disproportionation of $[H_3Ru_3(COMe)(CO)_6(PPh_3)_3]^{1+}$, $k_{12}$ is the rate constant for electron transfer (0.2 $M^{-1}$ $s^{-1}$ at 294 K), $k_{11}$ is the 47e/48e self-exchange rate constant, $k_{22}$ is the 47e/46e self-exchange rate constant, and $K_{12}$ is the disproportionation equilibrium constant ($E_2 - E_1$ 0.37 V, $K_{12}$ $4.3 \times 10^{-7}$). The values of $k_{11}$ can be estimated. The electrochemical reversibility of the 48-e/47-e oxidation implies a value of $k_{11}$ comparable to that of ferrocene/ferrocenium ($6 \times 10^6$ $M^{-1}$ $s^{-1}$ in acetonitrile) and we have previously used digital simulations to estimate the $[H_3Ru_3(COMe)(CO)_6(ax\text{-}PPh_3)_3]^{1+}/H_3Ru_3(COMe)(CO)_6(ax\text{-}PPh_3)_2(eq\text{-}PPh_3)$ electron exchange rate constant as $2 \times 10^5$ $M^{-1}$ $s^{-1}$ (the reverse rate constant is then $5 \times 10^3$ $M^{-1}$ $s^{-1}$); therefore a reasonable estimate of $k_{11}$ is $10^5$–$10^6$ $M^{-1}$ $s^{-1}$. Using these data, $k_{22}$ is estimated as ca. 0.4–4 $M^{-1}$ $s^{-1}$. The theory also expresses the activation free energy for electron transfer as Eq. (7):

$$\Delta G^{\ddagger} = (Z_D Z_A e^2 f/\varepsilon r_{DA}) + 0.25\lambda\ (1 + \Delta G'^0/\lambda)^2 \quad (7)$$

In this equation, $Z_D$ and $Z_A$ are the charges on the donor and acceptor, $e$ is the charge on the electron, $f$ is the ionic strength factor (taken to be 1), $\varepsilon$ is the dielectric constant for the solvent (8.9 for dichloromethane), $r_{DA}$ is the distance between donor and acceptor in the activated complex (taken as 10 Å), $\lambda$ is the reorganization energy required, and $G'^0$ is the free energy of the reaction, corrected for work. The reorganization energy can be estimated for the 47e/48e self-exchange (the first term is 0 and $\Delta G'^0 = 0$) as 155–175 kJ $mol^{-1}$. Assuming the same reorganization energy for the 47e/46e couple, the self-exchange rate constant $k_{22}$ is estimated to be 0.3–2 $M^{-1}$ $s^{-1}$. This analysis shows that the slower rate constant for the 47e/46e couple can be largely accounted for by the cationic charges of both species. Thus the data are consistent with rate-determining outer-sphere electron transfer, with the slow rate due to the large reorganization energy arising from electron transfer from one half-filled bonding orbital to another, and the cationic charge on donor and acceptor.

Faster decomposition occurs upon addition of large quantities of acetonitrile and small quantities of chloride. Addition of acetonitrile or chloride to the electrochemical experiments causes the 47-e/46-e anodic peak to shift in a cathodic direction, but has little effect upon the 48-e/47-e oxidation potential. The participation of these reagents reduces the contribution of the first term in Eq. (7), and also increases the disproportionation equilibrium constant, thus increasing the rate. We can rule out direct nucleophile-induced electron transfer since the $PPh_3$ effect is so small and since nucleophiles such as pyridine give very little rate enhancement. Chloride is a special case. Not only does added chloride dramatically increase the rate, but the 48-e product is formed in 66% yield. In dichloromethane solution, chloride is undoubtedly tightly ion-paired to the 47-e cations and can stabilize the 46-e product via coordination.

All other 47-e clusters examined by EPR also display second-order kinetics for decomposition. Decomposition of $[H_3Ru_3(COMe)(CO)_7(PPh_3)_2]^{1+}$ displays a second-order dependence in 47-e cluster concentration. Decomposition of $[H_3Ru_3(CSEt)(CO)_6(PPh_3)_3]^{1+}$ displays a second-order dependence in 47-e cluster concentration, with a second-order rate constant about the same as that for $[H_3Ru_3(COMe)(CO)_6(PPh_3)_3]^{1+}$, and decomposition in the presence of $PPh_3$ has been reported to form the purported 46-e $[H_3Ru_3(CO)_6$-

Table 6
Disproportionation equilibrium constants based upon the difference between first and second 1-e anodic peak potentials $E_{p,a1} - E_{p,a2}$

| 47-e cluster | $K_{disp}$ |
|---|---|
| $[H_3Ru_3(COMe)(CO)_7(PPh_3)_2]^{1+}$ | $2 \times 10^{-4}$ |
| $[H_3Ru_3(COMe)(CO)_6(PPh_3)_3]^{1+}$ | $9 \times 10^{-5}$ |
| $[H_3Ru_3(CNMeBz)(CO)_6(PPh_3)_3]^{1+}$ | $4 \times 10^{-7}$ |
| $[H_3Ru_3(CSEt)(CO)_6(PPh_3)_3]^{1+}$ | $8 \times 10^{-8}$ |
| $[H_3Ru_3(CPh)(CO)_6(PPh_3)_3]^{1+}$ | $2 \times 10^{-8}$ |

These represent lower limits

$(CS)(PPh_3)_3]^{1+}$ ($EtPPh_3^{1+}$ is however not a product of this reaction) [6]. Because of the identical NMR spectra observed for this decomposition product and for $[H_3Ru_3(CO)_7(PPh_3)_3]^{1+}$ we cannot rule the latter out as the true identity of the reaction product, but the 46-e species formed from $[H_3Ru_3(CSEt)(CO)_6(PPh_3)_3]^{1+}$ is much less stable than $[H_3Ru_3(CO)_7(PPh_3)_3]^{1+}$, suggesting that the two are in fact different compounds. The rate of the decomposition is increased by adding $PPh_3$, by a factor similar to that found for $[H_3Ru_3(COMe)(CO)_6(PPh_3)_3]^{1+}$. Since all of these exhibit second-order rate laws and ca. 50% recovery of the 48-e precursor, and reasonably similar rate constants, we propose that all of these reactions proceed through a rate-determining disproportionation step, with rapid decomposition of the 46-e product either by fragmentation, or in the cases of $[H_3Ru_3(COMe)(CO)_6(PPh_3)_3]^{2+}$ and $[H_3Ru_3(CSEt)(CO)_6(PPh_3)_3]^{2+}$, rapid follow-up loss of methyl cation or ethyl cation via attack by nucleophiles such as $PPh_3$.

The relative rates of decomposition, in the absence of $PPh_3$, at 294 K decrease in the series:

$[H_3Ru_3(CPh)(CO)_6(PPh_3)_3]^{1+}$ (fast)

$> H_3Ru_3(COMe)(CO)_7(PPh_3)_2$ (0.6 $M^{-1}$ $s^{-1}$)

$> [H_3Ru_3(COMe)(CO)_6(PPh_3)_3]^{1+}$ (0.16 $M^{-1}$ $s^{-1}$)

$\sim [H_3Ru_3(CSEt)(CO)_6(PPh_3)_3]^{1+}$ (0.12 $M^{-1}$ $s^{-1}$)

$> [H_3Ru_3(CNMeBz)(CO)_6(PPh_3)_3]^{1+}$ (slow)

and

$H_3Ru_3(COMe)(CO)_8(PPh_3)$ (ca 150–1500 $M^{-1}$ $s^{-1}$)

$> H_3Ru_3(COMe)(CO)_7(PPh_3)_2$

$> [H_3Ru_3(COMe)(CO)_6(PPh_3)_3]^{1+}$

These relative rates do not correlate appreciably with the driving force for the (unfavorable) disproportionation (which is almost unaffected by ligands or substituent, as shown by the near unity slope of the plot in Fig. 6); rather, they correlate with the oxidation potential, the more unstable the higher oxidation states, the faster the electron transfer. The larger rates must be associated with smaller reorganization energies since the disproportionation equilibrium constants are likely to be similar.

Although it is frequently assumed that reorganization energies are nearly the same within a related series of compounds, there is precedent for correlation of self-exchange rate constants with electrochemical potential. Self-exchange electron transfer rate constants for a series of substituted arenediazionium salts display a linear Hammett correlation with the $\sigma$ values of the substituent ($\rho$ +4.7) and a similar linear correlation of $\ln k_{ex}$ with polarographic half-wave reduction potentials. The unusually large variation in self-exchange rate constants was attributed to the high barriers for electron transfer ($\lambda$ 330–370 kJ $mol^{-1}$) [22].

The mechanism of decomposition of 47-e $[H_3Ru_3(CX)(CO)_{9-n}L_n]^{1+}$ is similar to the EC second-order disproportionation mechanism found for oxidative cleavage of the metal–metal bond in $[M_2(CO)_{10}]^{2-}$ (M = Cr, Mo, W), which was investigated by chronocoulometry [4]. The key step in this mechanism is slow disproportionation of $[M_2(CO)_{10}]^{1-}$ via outer sphere electron transfer, forming $[M_2(CO)_{10}]^{2-}$ and $M(CO)_5(THF)$. It was noted that there was no appreciable enhancement of the rate due to added nucleophiles. Phillips and Trogler attributed the relative stability of $[M_2(CO)_{10}]^{1-}$ toward nucleophilic attack to shielding of the SOMO, a M–M $\sigma$ bonding orbital, by axial CO ligands. The 47-e clusters $[H_3Ru_3(COMe)(CO)_{9-n}L_n]^{1+}$ are also relatively unreactive toward nucleophiles, for a similar reason. The main difference is that the electron transfer is 2–3 orders of magnitude slower.

## 4. Conclusions

Decomposition of the 47-e clusters $[H_3Ru_3(COMe)(CO)_{9-n}L_n]^{1+}$ proceeds by rate-determining disproportionation, regenerating stable 48-e $H_3Ru_3(COMe)(CO)_{9-n}L_n$ and very unstable 46-e $[H_3Ru_3(COMe)(CO)_{9-n}L_n]^{2+}$. The 46-e clusters are transformed into new species, which in some cases can be reduced back to the 48-e cluster at high scan rates, but mostly these decompose rapidly to uncharacterized products. In the presence of $PPh_3$ the 47-e $[H_3Ru_3(COMe)(CO)_6(PPh_3)_3]^{1+}$ decomposes to the 48-e $H_3Ru_3(COMe)(CO)_6(PPh_3)_3$, 46-e $[H_3Ru_3(CO)_7(PPh_3)_3]^{1+}$ and $MePPh_3^{1+}$. The rate law for this decomposition shows a very small dependence on $PPh_3$ concentration. The slow rate of disproportionation is a consequence of the fact that the electron transfer involves transfer of an electron from one half-filled bonding orbital to another half-filled bonding orbital. Similar ligand additivity relations apply to both 48-e/47-e and 47-e/46-e redox couples.

## 5. Supplementary material information available from the authors

Supplementary material is available from the authors upon request. Electrochemical data from Ref. [6] used for Figs. 3 and 6 and kinetic data for disproportionation reactions; electron density contour maps for the face plane for (a) $H_3Ru_3(CMe)(CO)_9$ and (b) $H_3Ru_3(COH)(CO)_9$; electron density map for $H_3Ru_3(COH)(CO)_8$(ax-$PH_3$) of the HOMO level in the plane defined by the methylidyne carbon, a Ru atom and the carbon of an equatorial carbonyl.

## Acknowledgements

Support for this work was provided by the Petroleum Research Fund. Some of the compounds used in this study were prepared by Dimitrios Kourouklis.

## References

[1] D. Astruc, Electron Transfer and Radical Processes in Transition-Metal Chemistry, VCH, New York, 1995.
[2] (a) T.L. Brown, in: W.C. Trogler (Ed.), Organometallic Radical Processes, Elsevier, Amsterdam, 1990, p. 67;
(b) J.K. Kochi, J. Organomet. Chem. 300 (1986) 139;
(c) D.R. Tyler, Prog. Inorg. Chem. 36 (1988) 125;
(d) N.G. Connelly, Chem. Soc. Rev. 18 (1989) 153;
(e) W.E. Geiger, Prog. Inorg. Chem. 33 (1985) 275.
[3] (a) W.C. Trogler, in: W.C. Trogler (Ed.), Organometallic Radical Processes, Elsevier, Amsterdam, 1990, p. 306;
(b) M. Sorlie, M. Tilset, Inorg. Chem. 34 (1995) 5199.
[4] J.R. Phillips, W.C. Trogler, Inorg. Chim. Acta 198–200 (1992) 633.
[5] M.R. Churchill, C.H. Lake, W.G. Feighery, J.B. Keister, Organometallics 10 (1991) 2384.
[6] W.G. Feighery, H. Yao, A.F. Hollenkamp, R.D. Allendoerfer, J.B. Keister, Organometallics 17 (1998) 872.
[7] H. Yao, R.D. McCargar, R.D. Allendoerfer, J.B. Keister, A.A. Low, J. Organomet. Chem. 568 (1998) 63.
[8] W. Paw, C.H. Lake, M.R. Churchill, J.B. Keister, Organometallics 14 (1995) 3768.
[9] (a) J.B. Keister, J.R. Shapley, D.A. Strickland, Inorg. Synth. 27 (1990) 196;
(b) J.B. Keister, T.L. Horling, Inorg. Chem. 19 (1980) 2304.
[10] M.R. Churchill, J.W. Ziller, D.M. Dalton, J.B. Keister, Organometallics 6 (1987) 806.
[11] Z.A. Rahman, L.R. Beanan, L.M. Bavaro, S.P. Modi, J.B. Keister, M.R. Churchill, J. Organomet. Chem. 263 (1984) 75.
[12] J.B. Keister, M.W. Payne, M.J. Muscatella, Organometallics 2 (1983) 219.
[13] (a) M.B. Hall, R.F. Fenske, Inorg. Chem. 11 (1972) 768;
(b) F. Herman, S. Skillman, Atomic Structure Calculations, Prentice-Hall, Englewood Cliffs, NJ, 1963;
(c) B.E. Bursten, R.J. Jensen, R.F. Fenske, J. Chem. Phys. 68 (1978) 3320.
[14] (a) A.B.P. Lever, Inorg. Chem. 29 (1990) 1271;
(b) H. Masui, A.B.P. Lever, Inorg. Chem. 32 (1993) 2199.
[15] C. Hansch, A. Leo, R.W. Taft, Chem. Rev. 91 (1991) 165.
[16] B.E. Bursten, M.R. Green, Prog. Inorg. Chem. 36 (1988) 393 and references therein.
[17] D.E. Sherwood, M.B. Hall Jr, Organometallics 1 (1982) 1519.
[18] (a) M.R. Churchill, L.R. Beanan, H.J. Wasserman, C. Bueno, Z.A. Rahman, J.B. Keister, Organometallics 2 (1983) 1179;
(b) M.R. Churchill, C.H. Lake, W.G. Feighery, J.B. Keister, Organometallics 10 (1991) 2384;
(c) N.J. Zhu, C. Lecompte, P. Coppens, J.B. Keister, Acta Crystallogr. B38 (1982) 1286;
(d) M.R. Churchill, T.P. Duggan, J.B. Keister, J.W. Ziller, Acta Crystallogr. C43 (1987) 203.
[19] L. Song, W.C. Trogler, J. Am. Chem. Soc. 114 (1992) 3355.
[20] J.T. McFadden, W.G. Feighery, J. Cluster Sci. 11 (2000) 373.
[21] J. Anhaus, H.C. Bajaj, R. van Eldik, L.R. Nevinger, J.B. Keister, Organometallics 8 (1989) 2903.
[22] M.P. Doyle, J.K. Guy, K.C. Brown, S.N. Mahapatro, C.M. VanZyl, J.R. Pladziewicz, J. Am. Chem. Soc. 109 (1987) 1536.
[23] K. Smith, C. Romming, M. Tilset, J. Am. Chem. Soc. 115 (1993) 8681.
[24] (a) D.W. Turner, Molecular Photoelectron Spectroscopy, Wiley, Chichester, UK, 1970;
(b) J.H.D. Eland, C.J. Danby, Z. Naturforsch. 23A (1968) 355;
(c) D.P. May, D.W. Turner, J. Chem. Soc. B (1968) 22.